*Inorg. Chem.* **2007**, *46*, 3492–3501


# Series of Trinuclear $Ni^{II}Ln^{III}Ni^{II}$ Complexes Derived from 2,6-Di(acetoacetyl)pyridine: Synthesis, Structure, and Magnetism

**Takuya Shiga,*,† Nobuhiro Ito,‡ Akiko Hidaka,‡ Hisashi Ōkawa,‡ Susumu Kitagawa,§ and Masaaki Ohba*,§**

*Department of Synthetic Chemistry and Biological Chemistry, Graduate School of Engineering, Kyoto University, Katsura, Nishikyo-ku, Kyoto 615-8510, Japan, Department of Chemistry, Faculty of Science, Kyushu University, Hakozaki, Higashi-ku 6-10-1, Fukuoka 812-8581, Japan*

Received October 7, 2006

Eighteen trinuclear $Ni^{II}_2Ln^{III}$ complexes of 2,6-di(acetoacetyl)pyridine ($H_2L$) (Ln = La–Lu except for Pm) were prepared by a "one-pot reaction" of $H_2L$, $Ni(NO_3)_2 \cdot 6H_2O$, and $Ln(NO_3)_3 \cdot nH_2O$ in methanol. X-ray crystallographic studies indicate that two $L^{2-}$ ligands sandwich two $Ni^{II}$ ions with the terminal 1,3-diketonate sites and one $Ln^{III}$ ion with the central 2,6-diacylpyridine site, forming the trinuclear $[Ni_2Ln(L)_2]$ core of a linear NiLnNi structure. The terminal Ni assumes a six-coordinate geometry together with methanol or water molecules, and the central Ln assumes a 10-coordinate geometry together with two or three nitrate ions. The $[Ni_2Ln(L)_2]$ core is essentially coplanar for large Ln ions (La, Ce, Pr, Nd) but shows a distortion with respect to the two $L^{2-}$ ligands for smaller Ln ions. Magnetic studies for the $Ni_2Ln$ complexes of diamagnetic $La^{III}$ and $Lu^{III}$ indicate an antiferromagnetic interaction between the terminal $Ni^{II}$ ions. A magnetic analysis of the $Ni_2Gd$ complex based on the isotropic Heisenberg model indicates a ferromagnetic interaction between the adjacent $Ni^{II}$ and $Gd^{III}$ ions and an antiferromagnetic interaction between the terminal $Ni^{II}$ ions. The magnetic properties of other $Ni_2Ln$ complexes were studied on the basis of a numerical approach with the $Ni_2La$ complex and analogous $Zn_2Ln$ complexes, and they indicated that the $Ni^{II}$–$Ln^{III}$ interaction is weakly antiferromagnetic for Ln = Ce, Pr, and Nd and ferromagnetic for Ln = Gd, Tb, Dy, Ho, and Er.

## Introduction

Magnetic studies of discrete heteronuclear metal complexes are important for understanding the spin-exchange mechanism between dissimilar metal ions and for appreciating the magnetic nature of molecular magnetic materials based on dissimilar metal ions.[1−10] Recently, magnetic studies on 3d−4f heteronuclear complexes have become important because of the increased attention devoted to 3d−4f-based magnetic materials. Many studies on 3d−4f mixed-metal complexes have been reported,[11−46] but most of the studies

* To whom correspondence should be addressed. E-mail: ohba@sbchem.kyoto-u.ac.jp (M.O.), shiga@chem.tsukuba.ac.jp (T.S.).

† Present address: Graduate School of Pure and Applied Sciences, University of Tsukuba, Tennodai 1-1-1, Tsukuba, Ibaraki 305-8571, Japan.

‡ Kyushu University.

§ Kyoto University.

(1) Kahn, O. *Struct. Bonding* **1987**, *68*, 89.
(2) Sinn, E.; Harris, C. M. *Coord. Chem. Rev.* **1969**, *4*, 391.
(3) Casellato, U.; Vigato, P. A. *Coord. Chem. Rev.* **1977**, *23*, 31.
(4) Zanello, P.; Tamburini, S.; Vigato, P. A.; Mazzocchin, G. A. *Coord. Chem. Rev.* **1987**, *77*, 165.
(5) Vigato, P. A.; Tamburini, S.; Fenton, D. E. *Coord. Chem. Rev.* **1990**, *106*, 25.
(6) Ōkawa, H.; Furutachi, H.; Fenton, D. E. *Coord. Chem. Rev.* **1998**, *174*, 51.
(7) Winpenny, R. E. P. *Chem. Soc. Rev.* **1998**, *27*, 447.
(8) Sakamoto, M.; Manseki, K.; Ōkawa, H. *Coord. Chem. Rev.* **2001**, *219−221*, 379.
(9) Benelli, C.; Gatteschi, D. *Chem. Rev.* **2002**, *102*, 2369.
(10) Kahn, O. *Acc. Chem. Res.* **2000**, *33*, 647.
(11) (a) Costes, J.-P.; Dahan, F.; Dupuis, A.; Laurent, J.-P. *Inorg. Chem.* **1997**, *36*, 4284. (b) Costes, J.-P.; Dahan, F.; Dupuis, A.; Laurent, J.-P. *Chem.—Eur. J.* **1998**, *4*, 1616. (c) Gheorghe, R.; Cucos, P.; Andruh, M.; Costes, J.-P.; Donnadieu, B.; Shova, S. *Chem.—Eur. J.* **2006**, *12*, 187.
(12) (a) Bencini, A.; Benelli, C.; Caneschi, A.; Carlin, R. L.; Dei, A.; Gatteschi, D. *J. Am. Chem. Soc.* **1985**, *107*, 8128. (b) Figuerola, A.; Diaz, C.; Ribas, J.; Tangoulis, V.; Sangregorio, C.; Gatteschi, D.; Maestro, M.; Mahia, J. *Inorg. Chem.* **2003**, *42*, 5274.
(13) (a) Andruh, M.; Ramade, I.; Codjovi, E.; Guillou, O.; Kahn, O.; Trombe, J. C. *J. Am. Chem. Soc.* **1993**, *115*, 1822. (b) Kahn, M. L.; Mathoniere, C.; Kahn, O. *Inorg. Chem.* **1999**, *38*, 3692. (c) Sutter, J.-P.; Kahn, M. L.; Kahn, O. *Adv. Mater.* **1999**, *11*, 863. (d) Kahn, M. L.; Sutter, J.-P.; Golhen, S.; Guionneau, P.; Ouahab, L.; Kahn, O.; Chasseau, D. *J. Am. Chem. Soc.* **2000**, *122*, 3413. (e) Kahn, M. L.; Lecante, P.; Verelst, M.; Mathoniere.; Kahn, O. *Chem. Mater.* **2000**, *12*, 3073. (f) Kahn, M. L.; Ballou, R.; Porcher, P.; Kahn, O.; Sutter, J.-P. *Chem.—Eur. J.* **2002**, *8*, 525. (g) Sutter, J.-P.; Kahn, M. L. In *Magnetism: Molecules to Materials*; Miller J. S., Drillon, M., Eds.; Wiley-VCH: New York, 2005; Vol. 5, p 161.
(14) Li, Y.-T.; Liao, D.-Z.; Jiang, Z.-H.; Wang, G.-L. *Polyhedron* **1995**, *14*, 2209.



10.1021/ic0619153 CCC: $37.00 
Published on Web 04/05/2007

are confined to the complexes of $Cu^{II}$ and $Gd^{III}$ ions. Bencini et al. first reported a ferromagnetic interaction between the adjacent $Cu^{II}$ and $Gd^{III}$ of trinuclear $Cu^{II}Gd^{III}Cu^{II}$ complexes, and subsequent studies have verified that the magnetic interaction in the $Cu^{II}-Gd^{III}$ pair is ferromagnetic, irrespective of the ligand nature.[12a]

However, magnetic interaction in the $Cu^{II}-Ln^{III}$ pair with paramagnetic $Ln^{III}$ except for $Gd^{III}$ has not been fully studied because of the first-order angular momentum in the Ln ions of the $4f^2-4f^6$ and $4f^8-4f^{13}$ electronic configurations. Kahn et al. have suggested that the magnetic nature in the $Cu^{II}-Ln^{III}$ pair is apparently antiferromagnetic for the Ln ions with $4f^1-4f^6$ configurations, whereas it is ferromagnetic for the Ln ions with $4f^8-4f^{13}$ configurations.[13b] To evaluate the magnetic interaction in $M^{II}Ln^{III}$ complexes, an empirical approach based on a comparison of analogous $M'^{II}Ln^{III}$ complexes of diamagnetic $M'^{II}$ was adopted. Kahn et al. studied the magnetic properties of $[M^{II}_3Ln^{III}_2]_n$ (M = Cu, Ni) compounds in comparison with analogous $[Zn^{II}_3Ln^{III}_2]_n$ compounds and observed the ferromagnetic nature of the $M^{II}-Tb^{III}$, $M^{II}-Dy^{III}$, and $M^{II}-Gd^{III}$ interactions.[13] Costes et al. examined the magnetic properties of dinuclear $Cu^{II}Ln^{III}$ complexes using analogous $Ni^{II}Ln^{III}$ ($S_{Ni} = 0$) complexes as the reference to observe that the $Cu^{II}-Ln^{III}$ interaction is antiferromagnetic for Ln = Ce, Nd, Sm, Tm, and Yb, whereas it is ferromagnetic for Ln = Gd, Tb, Dy, Ho, and Er.[11a] They demonstrated the significance and utility of the empirical approach based on systematic synthesis to evaluate the magnetic interaction between $Cu^{II}$ and $Ln^{III}$ ions. Previously, we studied the magnetic properties of a series of $Cu^{II}_2Ln^{III}$ complexes of a linear $Cu^{II}Ln^{III}Cu^{II}$ structure, in comparison with analogous $Zn_2$-Ln complexes, and observed that the $Cu^{II}-Ln^{III}$ interaction is antiferromagnetic for Ln = Ce, Pr, and Sm but ferromagnetic for Ln = Gd, Tb, Dy, Ho, and Er.[17a] These studies indicate that the magnetic interaction in the $Cu^{II}-Tb^{III}$, $Cu^{II}-Dy^{III}$, and $Cu^{II}-Gd^{III}$ pairs is apparently ferromagnetic, but there are some inconsistencies among these studies concerning the $Cu^{II}-Ln^{III}$ interaction for other Ln ions.

To systematically examine the magnetic interaction in 3d–4f compounds further, a series of $Ni^{II}_2Ln^{III}$ complexes of 2,6-di(acetoacetyl)pyridine ($H_2L$) were prepared in this work. The complexes crystallized in four different types: $[Ni_2Ln(L)_2(NO_3)_2(MeOH)_4]NO_3\cdot MeOH$ (type A: Ln = La (**1**), Ce (**2**), Pr (**3**), Nd (**4**), Sm (**5-A**), Eu (**6-A**), Gd (**7-A**)); $[Ni_2Ln(L)_2(NO_3)_2(H_2O)_2(MeOH)_2]NO_3\cdot 2H_2O\cdot MeOH$ (type B: Ln = Sm (**5-B**), Eu (**6-B**), Gd (**7-B**)); $[Ni_2Ln(L)_2(NO_3)_3(MeOH)_4]$ (type C: Ln = Gd (**7-C**), Tb (**8**), Dy (**9**)); and $[Ni_2Ln(L)_2(NO_3)_2(H_2O)(MeOH)_3]NO_3\cdot Et_2O\cdot MeOH$ (type D: Ln = Ho (**10**), Er (**11**), Tm (**12**), Yb (**13**), Lu (**14**)). All of the complexes were structurally characterized, and the $[Ni_2Ln(L)_2]$ core structures of types A–D are discussed in terms of the size of the Ln ions. Our main focuses are the systematic synthesis of the $Ni^{II}-Ln^{III}$ compounds and the elucidation of their magnetic interaction with respect to the electronic structure of the Ln ion.


(15) (a) Kido, T.; Nagasato, S.; Sunatsuki, Y.; Matsumoto, N. *Chem. Commun.* **2000**, 2113. (b) Yamaguchi, T. Sunatsuki, Y.; Kojima, M.; Akashi, H.; Tsuchimoto, M.; Re, N.; Osa, S.; Matsumoto, N. *Chem. Commun.* **2004**, 1048. (c) Osa, S.; Kido, T.; Matsumoto, N.; Re, N.; Pochaba, A.; Mrozinski, J. *J. Am. Chem. Soc.* **2004**, *126*, 420.

(16) (a) Sasaki, M.; Horiuchi, H.; Kumagai, M.; Sakamoto, M.; Sakiyama, H.; Nishida, Y.; Sadaoka, Y.; Ohba, M.; Ōkawa, H. *Chem. Lett.* **1998**, 911. (b) Kondoh, N.; Shimizu, Y.; Kurihara, M.; Sakiyama, H.; Sakamoto, M.; Nishida, Y.; Sadaoka, Y.; Ohba, M.; Ōkawa, H. *Bull. Chem. Soc. Jpn.* **2003**, *76*, 1007.

(17) (a) Shiga, T.; Ohba, M.; Ōkawa, H. *Inorg. Chem.* **2004**, *43*, 4435. (b) Shiga, T.; Ohba, M.; Ōkawa, H. *Inorg. Chem. Commun.* **2003**, *6*, 15. (c) Ohba, M.; Ohtsubo, N.; Shiga, T.; Sakamoto, M.; Ōkawa, H. *Polyhedron* **2003**, *22*, 1905.

(18) (a) Ma, B.-Q.; Sun, H.-L.; Gao, S. *Chem. Commun.* **2005**, 2336. (b) Cai, Y.-P.; Li, G.-B.; Zhan, Q.-G.; Sun, F.; Zhang, J.-G.; Gao, S.; Xu, A.-W. *J. Solid State Chem.* **2005**, *178*, 3729.

(19) (a) Du, B.; Meyers, E. A.; Shore, S. G. *Inorg. Chem.* **2000**, *39*, 4639. (b) Du, B.; Meyers, E. A.; Shore, S. G. *Inorg. Chem.* **2001**, *40*, 4353. (c) Du, B.; Ding, E.; Meyers, E. A.; Shore, S. G. *Inorg. Chem.* **2001**, *40*, 3637. (d) Liu, J.; Knoeppel, D. W.; Liu, S.; Meyers, E. A.; Shore, S. G. *Inorg. Chem.* **2001**, *40*, 2842. (e) Liu, S. M., Edward, A.; Shore, S. G. *Angew. Chem., Int. Ed.* **2002**, *41*, 3609. (f) Plecnik, C. E.; Liu, S.; Shore, S. G. *Acc. Chem. Res.* **2003**, *36*, 499.

(20) Blake, A. J.; Milne, P. E. Y.; Thornton, P.; Winpenny, R. E. P. *Angew. Chem., Int. Ed. Engl.* **1991**, *30*, 1139.

(21) Wang, S.; Pang, Z.; Smith, K. D. L.; Hua, Y.-s.; Deslippe, C.; Wagner, M. J. *Inorg. Chem.* **1995**, *34*, 908.

(22) Chen, X.-M.; Aubin, S. M. J.; Wu, Y.-L.; Yang, Y.-S.; Mak, T. C. W.; Hendrickson, D. N. *J. Am. Chem. Soc.* **1995**, *117*, 9600.

(23) Decurtins, S.; Gross, M.; Schmalle, H. W.; Ferlay, S. *Inorg. Chem.* **1998**, *37*, 2443.

(24) Liang, Y.; Hong, M.; Su, W.; Cao, R.; Zhang, W. *Inorg. Chem.* **2001**, *40*, 4574.

(25) Gheorghe, R.; Andruh, M.; Muller, A.; Schmidtmann, M. *Inorg. Chem.* **2002**, *41*, 5314.

(26) Rizzi, A. C.; Calvo, R.; Baggio, R.; Garland, M. T.; Pena, O.; Perec, M. *Inorg. Chem.* **2002**, *41*, 5609.

(27) He, Z.; He, C.; Gao, E.-Q.; Wang, Z.-M.; Yang, X.-F.; Liao, C.-S.; Yan, C.-H. *Inorg. Chem.* **2003**, *42*, 2206.

(28) Pradhan, R.; Desplanches, C.; Guionneau, P.; Sutter, J.-P. *Inorg. Chem.* **2003**, *42*, 6607.

(29) Xu, Z.; Read, P. W.; Hibbs, D. E.; Hursthouse, M. B.; Malik, K. M. A.; Patrick, B. O.; Rettig, S. J.; Seid, M.; Summers, D. A.; Pink, M.; Thompson, R. C.; Orvig, C. *Inorg. Chem.* **2000**, *39*, 508.

(30) Bayly, S. R.; Xu, Z.; Patrick, B. O.; Rettig, S. J.; Pink, M.; Thompson, R. C.; Orvig, C. *Inorg. Chem.* **2003**, *42*, 1576.

(31) Figuerola, A.; Diaz, C.; Ribas, J.; Tangoulis, V.; Granell, J.; Lloret, F.; Mahia, J.; Maestro, M. *Inorg. Chem.* **2003**, *42*, 641.

(32) Piguet, C.; Edder, C.; Rigault, S.; Bernardinelli, G.; Bunzli, J.-C. G.; Hopfgartner, G. *Dalton Trans.* **2000**, 3999.

(33) Edder, C.; Piguet, C.; Bunzli, J.-C. G.; Hopfgartner, G. *Chem.—Eur. J.* **2001**, *7*, 3014.

(34) Avecilla, F.; Platas-Iglesias, C.; Rodriguez-Cortinas, R.; Guillemot, G.; Bunzli, J.-C. G.; Brondino, C. D.; Geraldes, C. F. G. C.; Blas, A. D.; Rodriguez-Blas, T. *Dalton Trans.* **2002**, 4658.

(35) Turta, C.; Prodius, D.; Mereacre, V.; Shova, S.; Gdaniec, M.; Simonov, Y. A.; Kuncser, V.; Filoti, G.; Caneschi, A.; Sorace, L. *Inorg. Chem. Commun.* **2004**, *7*, 576.

(36) Atria, A. M.; Moreno, Y.; Spodine, E.; Garland, M. T.; Baggio, R. *Inorg. Chim. Acta* **2002**, *335*, 1.

(37) Paulovic, J.; Cimpoesu, F.; Ferbinteanu, M.; Hirao, K. *J. Am. Chem. Soc.* **2004**, *126*, 3321.

(38) Sanz, J. L.; Ruiz, R.; Gleizes, A.; Lloret, F.; Faus, J.; Julve, M.; Borras-Almenar, J. J.; Journaux, Y. *Inorg. Chem.* **1996**, *35*, 7384.

(39) Chen, X.-M.; Wu, Y.-L.; Yang, Y.-Y.; Aubin, S. M. J.; Hendrickson, D. N. *Inorg. Chem.* **1998**, *37*, 6186.

(40) (a) Sanada, T.; Suzuki, T.; Yoshida, T.; Kaizaki, S. *Inorg. Chem.* **1998**, *37*, 4712. (b) Sanada, T.; Suzuki, T.; Kaizaki, S. *J. Chem. Soc., Dalton Trans.* **1998**, 959.

(41) Stemmler, A. J.; Kampf, J. W.; Kirk, M. L.; Atasi, B. H.; Pecoraro, V. L. *Inorg. Chem.* **1999**, *38*, 2807.

(42) Madalan, A. M.; Roesky, H. W.; Andruh, M.; Noltemeyer, M.; Stanica, N. *Chem. Commun.* **2002**, 1638.

(43) Tang, J.-K.; Li, Y.-Z.; Wang, Q.-L.; Gao, E.-Q.; Liao, D.-Z.; Jiang, Z.-H.; Yan, S.-P.; Cheng, P.; Wang, L.-F.; Wang, G.-L. *Inorg. Chem.* **2002**, *41*, 2188.

(44) Nishihara, S.; Akutagawa, T.; Hasegawa, T.; Nakamura, T. *Inorg. Chem.* **2003**, *42*, 2480.

(45) Akine, S.; Matsumoto, T.; Taniguchi, T.; Nabeshima, T. *Inorg. Chem.* **2005**, *46*, 8091.

(46) Yukawa.Y.; Aromi, G.; Igarashi, S.; Ribas, J.; Zvyagin, S. A.; Krzystek, J. *Angew. Chem., Int. Ed.* **2005**, *44*, 1997.

**Table 1.** Yield and Elemental Analysis for $[Ni_2Ln(L)_2(NO_3)_3(H_2O)_4]\cdot nH_2O$ (**1′**−**14′**)

| $[Ni_2Ln(L)_2(NO_3)_3(H_2O)_4]\cdot nH_2O$ | | | | | | | | | | |
|---|---|---|---|---|---|---|---|---|---|---|
| complex | Ln | *n* | yield (%) | %C found (calcd) | %H found (calcd) | %N found (calcd) | %Ni found (calcd) | IR data ($cm^{-1}$) | | |
| (**1′**) | La | 3 | 75 | 29.38 (29.49) | 3.32 (3.43) | 6.74 (6.61) | 10.97 (11.09) | 1613 | 1593 | 1385 |
| (**2′**) | Ce | 2 | 70 | 30.01 (29.97) | 3.20 (3.29) | 6.85 (6.72) | 11.21 (11.26) | 1613 | 1594 | 1385 |
| (**3′**) | Pr | 3 | 76 | 29.64 (29.44) | 3.21 (3.42) | 6.67 (6.60) | 11.40 (11.07) | 1611 | 1595 | 1385 |
| (**4′**) | Nd | 3 | 73 | 29.40 (29.34) | 3.26 (3.41) | 6.61 (6.58) | 10.77 (11.03) | 1609 | 1596 | 1385 |
| (**5′**) | Sm | 4 | 55 | 28.78 (28.69) | 3.45 (3.52) | 6.50 (6.43) | 10.93 (10.79) | 1613 | 1595 | 1385 |
| (**6′**) | Eu | 4 | 57 | 28.78 (28.65) | 3.29 (3.51) | 6.51 (6.43) | 10.35 (10.77) | 1613 | 1596 | 1385 |
| (**7′**) | Gd | 4 | 46 | 28.64 (28.51) | 3.40 (3.50) | 6.45 (6.39) | 10.88 (10.72) | 1615 | 1596 | 1385 |
| (**8′**) | Tb | 2 | 84 | 29.49 (29.44) | 3.17 (3.23) | 6.64 (6.60) | 11.01 (11.07) | 1613 | 1596 | 1385 |
| (**9′**) | Dy | 2 | 82 | 29.12 (29.34) | 3.25 (3.22) | 6.61 (6.58) | 11.04 (11.03) | 1614 | 1596 | 1386 |
| (**10′**) | Ho | 2 | 88 | 29.27 (29.27) | 3.21 (3.21) | 6.63 (6.56) | 10.71 (11.00) | 1613 | 1597 | 1385 |
| (**11′**) | Er | 2 | 81 | 29.09 (29.21) | 3.17 (3.21) | 6.57 (6.55) | 10.74 (10.98) | 1614 | 1596 | 1385 |
| (**12′**) | Tm | 2 | 83 | 29.02 (29.16) | 3.22 (3.20) | 6.55 (6.54) | 10.60 (10.96) | 1613 | 1597 | 1385 |
| (**13′**) | Yb | 2 | 75 | 28.84 (29.05) | 3.24 (3.19) | 6.51 (6.51) | 10.86 (10.92) | 1614 | 1597 | 1385 |
| (**14′**) | Lu | 2 | 82 | 28.76 (29.00) | 3.21 (3.18) | 6.48 (6.50) | 11.04 (10.90) | 1614 | 1597 | 1385 |

## Materials

2,6-Di(acetoacetyl)pyridine ($H_2L$) was prepared according to the literature method.[47] Other chemicals were of reagent grade and were purchased from commercial sources.

**$Ni_2Ln$ Complexes.** A solution of $H_2L$ (1.0 mmol) and triethylamine (1.0 mmol) in methanol (10 $cm^3$) was added to a solution of $Ni(NO_3)_2\cdot 6H_2O$ (1.0 mmol) and $Ln(NO_3)_3\cdot nH_2O$ (0.5 mmol) in hot methanol (10 $cm^3$), and the mixture was stirred for a while. The reaction mixture was slowly evaporated at ambient temperature to afford green crystals of $[Ni_2Ln(L)_2(NO_3)_2(MeOH)_4]NO_3\cdot MeOH$ (type A: Ln = La (**1**), Ce (**2**), Pr (**3**), Nd (**4**), Sm (**5-A**), Eu (**6-A**), Gd (**7-A**)); $[Ni_2Ln(L)_2(NO_3)_2(H_2O)_2(MeOH)_2]NO_3\cdot 2H_2O\cdot MeOH$ (type B: Ln = Sm (**5-B**), Eu (**6-B**), Gd (**7-B**)); and $[Ni_2Ln(L)_2(NO_3)_3(MeOH)_4]$ (type C: Ln = Gd (**7-C**), Tb (**8**), Dy (**9**)). The $Ni_2Ln$ complexes of heavy Ln ions, $[Ni_2Ln(L)_2(NO_3)_2(H_2O)(MeOH)_3]NO_3\cdot Et_2O\cdot MeOH$ (type D: Ln = Ho (**10**), Er (**11**), Tm (**12**), Yb (**13**), Lu (**14**)), were prepared as green crystals when the reaction mixture was diffused with diethyl ether. The complexes were converted into $[Ni_2Ln(L)_2(NO_3)_3(H_2O)_4]\cdot nH_2O$ (**1′**−**14′**) on desiccating at 100 °C in vacuo and exposing to air at room temperature. The analytical data of **1′**−**14′** are summarized in Table 1.

**$Zn_2Ln$ Complexes.** The $Zn_2Ln$ complexes, $[Zn_2Ln(L)_2(NO_3)_3(H_2O)_2]\cdot nH_2O$ (Ln = La−Er except for Pm; $n$ = 0 or 1), were prepared by the method described previously.[17a]

**X-ray Structure Determination.** All measurements were made on a Rigaku Raxis-Rapid Imaging plate diffractometer with graphite-monochromated Mo Kα radiation ($\lambda$ = 0.71069 Å). Indexing was performed from two or three oscillations, which were exposed for 1.0−10.0 min. The camera radius was 127.40 mm. The data were collected at a temperature of −90 ± 1 °C to a maximum $2\theta$ value of 55.0°. A total of 44−75 images, corresponding to 220.0°−225.0° oscillation angles, were collected with two different goniometer settings. Exposure time was 0.5−2.0 min per degree. Readout was performed in the 0.100 mm pixel mode. Data were processed by the PROCESS-AUTO program package. A symmetry-related absorption correction using the program ABSCOR was applied.[48] The data were corrected for Lorentz and polarization effects.

All calculations were performed using the teXsan[49] crystallographic software package from Molecular Structure Corporation. Hydrogen atoms were included but not refined. Crystallographic data for the structures reported here have been deposited at the Cambridge Crystallographic Data Centre (CCDC) as supplementary publication numbers CCDC 623149−623166.

**Magnetic Measurements.** Magnetic measurements for **1′**−**14′** were carried out on powdered samples with a Quantum Design SQUID MPMS-5XL magnetometer in the temperature range of 2−300 K and under an applied magnetic field of 500 Oe. Field dependencies of magnetization were measured at 2 K under an applied field up to 50 kOe. Diamagnetic corrections were applied using Pascal's constants. Effective magnetic moments were calculated by the equation $\mu_{eff} = (8\chi_M T)^{1/2}$.

**Elemental Analyses and Spectroscopic Measurements.** Elemental analyses of C, H, and N were performed at the Elemental Analysis Service Center of Kyushu University. Nickel analyses were made on a Shimadzu AA−680 atomic absorption/flame emission spectrophotometer. Infrared spectra were measured on KBr disks with a Perkin-Elmer Spectrum BX FTIR system.

(47) Fenton, D. E.; Tate, J. R.; Casellato, U.; Tamburini, S.; Vigato, P. A.; Vidali, M. *Inorg. Chim. Acta* **1984**, *83*, 23.

(48) *Program for Absorption Correction*; Rigaku Corp.: Tokyo, Japan, 1995.

(49) *teXsan: Crystal Structure Analysis Package*; Molecular Structure Corporation: The Woodlands, TX, 1985 and 1999.

## Results and Discussion

**Preparation.** It is known from our previous work that the ligand $H_2L$ has a specificity to accommodate the $Cu^{II}$ ion with the terminal 1,3-diketonate site and the $Ln^{III}$ ion with the central 2,6-diacylpyridine site, producing trinuclear $Cu_2$-Ln complexes of a linear CuLnCu structure. In this study, a series of $Ni_2Ln$ complexes was produced by a one-pot reaction of $H_2L$, $Ni(NO_3)_2{\cdot}6H_2O$, and $Ln(NO_3)_3{\cdot}nH_2O$ in methanol. The $Ni_2Ln$ complexes of light Ln ions could be easily obtained, but the yield decreased in complexes of heavier Ln ions. In practice, **1**−**9** (Ln = La−Dy) were crystallized on slow evaporation of each reaction solution, but **10**−**14** (Ln = Ho−Lu) could not be obtained by this method. Eventually, **10**−**14** were obtained by diffusing diethyl ether into each reaction solution. **5** and **6** crystallized in two different forms (A and B), and **7** crystallized in three different forms (A, B, and C). The different crystalline forms of **5**, **6**, and **7** were manually separated and characterized by X-ray crystallography, as discussed below. Type A was the main product in the synthesis of **5** and **6**, and type C was the main product in the synthesis of **7**.

The crystals of **1**−**14** were efflorescent, and the coordinated methanol molecules and the lattice solvent molecules were replaced with atmospheric water. The resulting aqua complexes, $[Ni_2Ln(L)_2(NO_3)_3(H_2O)_4]{\cdot}nH_2O$ (**1′**−**14′**), retained the linear trinuclear core structure and were used for magnetic studies. All of the compounds showed characteristic IR bands assigned to two $\beta$-diketonate-chelate sites and nitrate ions (Table 1).

**Description of Structure.** X-ray crystallographic results for **1**−**14** demonstrated that two $L^{2-}$ ligands sandwich two $Ni^{II}$ ions with the terminal 1,3-diketonate sites and one $Ln^{III}$ ion with the central 2,6-diacylpyridine site, affording a $[Ni_2Ln(L)_2]$ core of a linear NiLnNi structure. The structures of the complexes are classified into four types, A−D, on the basis of the space group and the molecular geometry (Scheme 1). Crystal parameters for selected complexes are given in Table 2. Structural characteristics of all of the complexes are summarized in Table 3. Crystal parameters and selected bond distances for all of the complexes are listed in Tables S1 and S2.

**Type A. $[Ni_2Ln(L)_2(NO_3)_2(MeOH)_4]NO_3{\cdot}MeOH$ (Ln = La (1), Ce (2), Pr (3), Nd (4), Sm (5-A), Eu (6-A), and Gd (7-A)).** This type crystallizes in the triclinic system with space group $P\bar{1}$. The structure of **7-A** is given in Figure 1 as an example. The asymmetric unit consists of each half of $[Ni_2Gd(L)_2(NO_3)_2(MeOH)_4]^+$, $NO_3^-$, and MeOH. The Gd ion is located at the inversion center. The $[Ni_2Gd(L)_2]$ core forms a near plane, affording an $N_2O_4$ hexagonal base for the Gd ion and an $O_4$ tetragonal base for the Ni ion. The Gd assumes a 10-coordinate geometry together with two didentate nitrate groups above and below the hexagonal base. The in-plane Gd−N and Gd−O(L) bond distances are 2.719 and 2.524 Å, respectively, and the axial Gd−O(nitrate) distance is 2.498 Å. Each Ni has a six-coordinate geometry with two methanol molecules at the axial sites. The bond distances between Ni and the inside oxygen atoms (Ni−O2 = 1.992(3) and Ni−O3* = 2.004(3) Å) are longer than those between Ni and the outside oxygen atoms (Ni−O1 = 1.981(3) and Ni−O4* = 1.976(3) Å), because the inside oxygen atoms are attracted by the central Gd ion. The average Ni-to-donor distance is 2.032 Å. The Ni−Gd and Ni−Ni* (*, symmetry operation $(-x, -y, -z)$) separations are 3.692 and 7.383 Å, respectively. One nitrate ion and one MeOH molecule are free from coordination and alternately occupy the crystallographically equivalent space with an occupancy factor of 0.5 in the lattice.

**Scheme 1.** Schematic Drawings of the Structures of Types A−D with Respect to the Exogenous Donor Groups

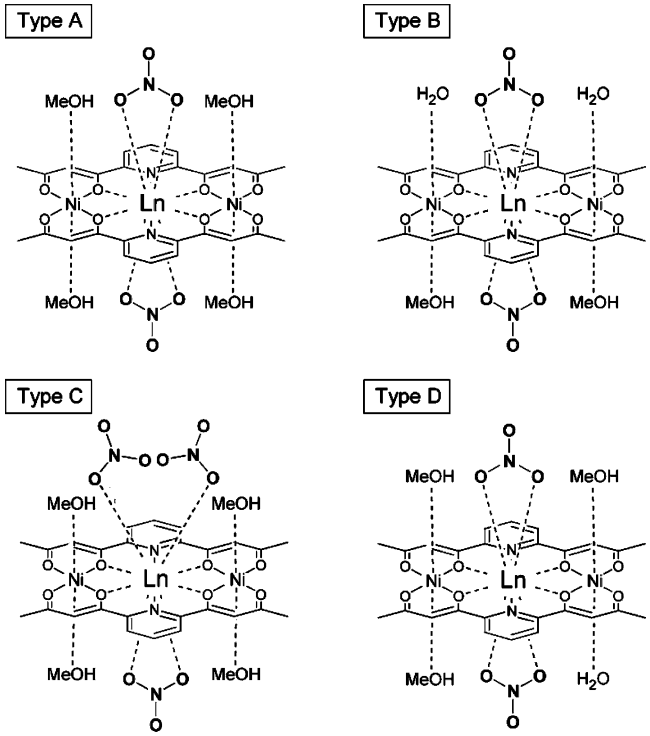


The structural characteristics of type A complexes are summarized in Table 3. The Ln−N, Ln−O(L), and Ln−O(nitrate) bond distances generally decrease in the order **1** > **2** > **3** > **4** > **5-A** > **6-A** > **7-A**, in accord with the lanthanide contraction. The average Ni−O distance varies from 2.025 to 2.032 Å. The Ni−Ln and Ni−Ni* separations are practically invariant with the Ln ions, because the trinuclear NiLnNi structure is fixed by two $L^{2-}$ ligands.

**Type B. $[Ni_2Ln(L)_2(NO_3)_2(H_2O)_2(MeOH)_2]NO_3{\cdot}2H_2O{\cdot}$ MeOH (Ln = Sm (5-B), Eu (6-B), Gd (7-B)).** This type crystallizes in the triclinic system with space group $P\bar{1}$. The structure of **7-B** is given in Figure 2. The asymmetric unit consists of one $[Ni_2Gd(L)_2(NO_3)_2(H_2O)_2(MeOH)_2]^+$ cation, one nitrate ion, two water molecules, and two MeOH molecules. The $[Ni_2Gd(L)_2]$ core shows a distortion with respect to two $L^{2-}$ ligands; the dihedral angle ($\phi_{Ln}$) defined by the two pyridine rings in the core is 24.6°. The two Ni atoms are not equivalent but have a similar six-coordinate geometry with one water and one MeOH molecule at the axial sites. The water molecule on Ni(1) and that on Ni(2) are situated cis with respect to the $[Ni_2Gd(L)_2]$ base.

**Table 2.** Crystal Parameters for Complexes **7-A**, **7-B**, **7-C**, and **14**

| | 7-A | 7-B | 7-C | 14 |
|---|---|---|---|---|
| formula | $C_{31}H_{38}N_5GdNi_2O_{22}$ | $C_{29}H_{42}N_5GdNi_2O_{24}$ | $C_{30}H_{38}N_5GdNi_2O_{21}$ | $C_{34}H_{50}N_5Ni_2LuO_{23}$ |
| fw | 1107.31 | 1119.32 | 1079.3 | 1189.16 |
| cryst color | blue | blue | green | green |
| cryst syst | triclinic | triclinic | monoclinic | triclinic |
| No. | $P\bar{1}$ (2) | $P\bar{1}$ (2) | $C2/c$ (15) | $P\bar{1}$ (2) |
| $a$ (Å) | 7.8220(4) | 7.9047(8) | 14.103(1) | 10.8349(7) |
| $b$ (Å) | 9.3686(5) | 16.786(2) | 17.2153(9) | 14.809(2) |
| $c$ (Å) | 14.4871(9) | 17.040(2) | 16.3096(8) | 16.448(2) |
| α (deg) | 92.321(3) | 68.804(6) | | 109.124(3) |
| $\beta$ (deg) | 104.321(3) | 78.224(4) | 99.328(3) | 100.140(3) |
| $\gamma$ (deg) | 91.211(2) | 78.643(4) | | 110.188(5) |
| $V$ (Å$^3$) | 1027.26(9) | 2044.8(3) | 3907.5(4) | 2212.4(4) |
| Z value | 1 | 2 | 4 | 2 |
| $T$ (°C) | −90 | −60 | −90 | −90 |
| $\lambda$ (Å) | 0.71069 | 0.71069 | 0.71069 | 0.71069 |
| $\mu$(Mo Kα) (cm$^{-1}$) | 25.97 | 26.14 | 27.26 | 31.47 |
| $D_c$ (g·cm$^{-3}$) | 1.790 | 1.818 | 1.835 | 1.785 |
| no. observations (all) | 4536 | 8742 | 4428 | 9811 |
| $R1$[a] ($I > 2.0\sigma(I)$) | 0.034 | 0.038 | 0.047 | 0.030 |
| $R$[b] (all obsd) | 0.056 | 0.064 | 0.085 | 0.049 |
| $R_w$[c] (all obsd) | 0.091 | 0.135 | 0.066 | 0.094 |
| GOF | 1.00 | 1.00 | 1.00 | 1.00 |

[a] $R1 = \Sigma||F_o| - |F_c||/\Sigma|F_o|$. [b] $R = \Sigma|F_o^2 - F_c^2|/\Sigma F_o^2$. [c] $R_w = [\Sigma[w(|F_o|^2 - |F_c|^2)^2]/\Sigma w|F_o^2|^2]^{1/2}$.

**Table 3.** Summary of Structural Characteristics of **1**−**14**

| complex | | intermetallic separation (Å) | | $\phi_{Ln}$[b] (deg) | $\phi_{Ni}$[c] (deg) | bond distance (Å) | | | | ionic radius of $Ln^{III}$ |
|---|---|---|---|---|---|---|---|---|---|---|
| | | Ni−Ln | Ni−Ni[a] | | | average Ni−O | Ln−N | Ln−$O_L$ | Ln−$O_{ax}$ | |
| $Ni_2La$ | (**1**) | 3.696 | 7.393 | 0 | 0 | 2.032 | 2.762 | 2.569 | 2.616 | 1.06 |
| $Ni_2Ce$ | (**2**) | 3.691 | 7.383 | 0 | 0 | 2.032 | 2.753 | 2.556 | 2.590 | 1.03 |
| $Ni_2Pr$ | (**3**) | 3.688 | 7.376 | 0 | 0 | 2.029 | 2.740 | 2.546 | 2.568 | 1.01 |
| $Ni_2Nd$ | (**4**) | 3.682 | 7.365 | 0 | 0 | 2.027 | 2.736 | 2.537 | 2.550 | 0.99 |
| $Ni_2Sm$ | (**5-A**) | 3.686 | 7.371 | 0 | 0 | 2.028 | 2.723 | 2.529 | 2.516 | 0.96 |
| $Ni_2Eu$ | (**6-A**) | 3.680 | 7.360 | 0 | 0 | 2.025 | 2.719 | 2.519 | 2.501 | 0.95 |
| $Ni_2Gd$ | (**7-A**) | 3.692 | 7.383 | 0 | 0 | 2.027 | 2.719 | 2.524 | 2.498 | 0.94 |
| $Ni_2Sm$ | (**5-B**) | 3.664 | 7.325 | 24.6 | 33.7 | 2.028 | 2.679 | 2.516 | 2.509 | 0.96 |
| $Ni_2Eu$ | (**6-B**) | 3.655 | 7.308 | 24.8 | 34.7 | 2.024 | 2.668 | 2.501 | 2.482 | 0.95 |
| $Ni_2Gd$ | (**7-B**) | 3.681 | 7.361 | 25.0 | 35.0 | 2.037 | 2.675 | 2.513 | 2.483 | 0.94 |
| $Ni_2Gd$ | (**7-C**) | 3.635 | 7.255 | 32.3 | 47.8 | 2.025 | 2.672 | 2.479 | 2.506 | 0.94 |
| $Ni_2Tb$ | (**8**) | 3.635 | 7.256 | 31.1 | 47.3 | 2.028 | 2.662 | 2.476 | 2.491 | 0.92 |
| $Ni_2Dy$ | (**9**) | 3.626 | 7.239 | 31.7 | 48.1 | 2.026 | 2.657 | 2.469 | 2.480 | 0.91 |
| $Ni_2Ho$ | (**10**) | 3.583 | 7.165 | 42.6 | 65.2 | 2.034 | 2.588 | 2.419 | 2.455 | 0.89 |
| $Ni_2Er$ | (**11**) | 3.585 | 7.168 | 42.8 | 65.5 | 2.033 | 2.584 | 2.413 | 2.444 | 0.88 |
| $Ni_2Tm$ | (**12**) | 3.580 | 7.160 | 43.0 | 66.0 | 2.036 | 2.583 | 2.408 | 2.438 | 0.87 |
| $Ni_2Yb$ | (**13**) | 3.576 | 7.151 | 43.4 | 66.7 | 2.039 | 2.579 | 2.403 | 2.441 | 0.86 |
| $Ni_2Lu$ | (**14**) | 3.569 | 7.137 | 43.6 | 67.0 | 2.034 | 2.571 | 2.395 | 2.416 | 0.85 |

[a] The values mean Ni−Ni* separation for types A and C (* indicates the symmetry operation $(-x, -y, -z)$ for type A, $(-x, y, -z + {}^1/_2)$ for type C), and Ni1−Ni2 separation for types B and D. [b] Distortion about Ln defined by the dihedral angle between two pyridine rings. [c] Distortion about Ni defined by the dihedral angle between the least-squares planes defined by four oxygen atoms of two 1,3-diketonate sites and Ni.

The structural characteristics of type B complexes are given in Table 3. The dihedral angle ($\phi_{Ln}$) varies from 24.6 to 25.0°. Because of this distortion, the in-plane Ln−N and Ln−O(L) bond distances of **5-B**, **6-B**, and **7-B** are shortened relative to those of **5-A**, **6-A**, and **7-A**, respectively. The average Ni−O distance falls in the range of 2.024−2.037 Å. The Ni−Ln and Ni(1)−Ni(2) separations of **5-B**, **6-B**, and **7-B** are also short, relative to those of **5-A**, **6-A**, and **7-A**, respectively.

**Type C. $[Ni_2Ln(L)_2(NO_3)_3(MeOH)_4]$ (Ln = Gd (7-C), Tb (8), Dy (9)).** This type crystallizes in the monoclinic system of space group $C2/c$. The structure of **7-C** is shown in Figure 3. The two Ni centers are equivalent and have a six-coordinate geometry together with two MeOH molecules at the axial sites. The Gd atom is located at the special equivalent position and has a 10-coordinate environment together with two unidentate nitrate groups and one didentate nitrate group. The $[Ni_2Gd(L)_2]$ core shows a distortion with respect to two $L^{2-}$ ligands; the dihedral angle ($\phi_{Ln}$) is 32.3°.

The structural characteristics of type C complexes are given in Table 3. Type C has a larger distortion in the trinuclear core compared with type B complexes; the $\phi_{Ln}$ value falls in the range of 31.1−32.3°. For of this reason, the Gd−N, Gd−O(L), Ni−Ln, and Ni−Ni' (', symmetry operation $(-x, y, -z + {}^1/_2)$) bond distances of **7-C** are shortened relative to those of **7-B**.

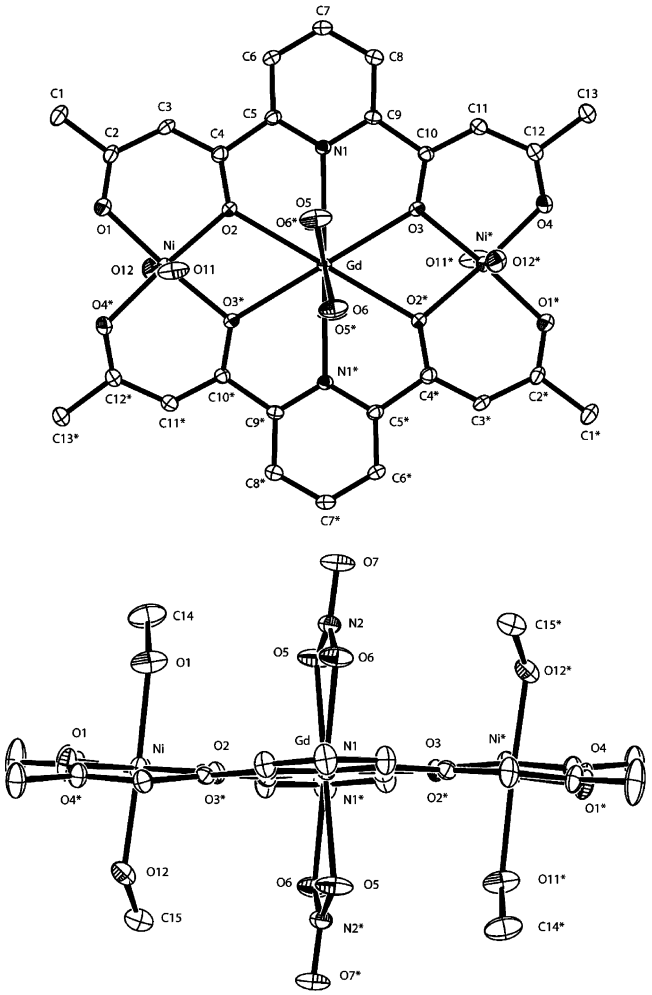


**Figure 1.** ORTEP drawings of $Ni_2Gd$ complex **7-A** (type A).

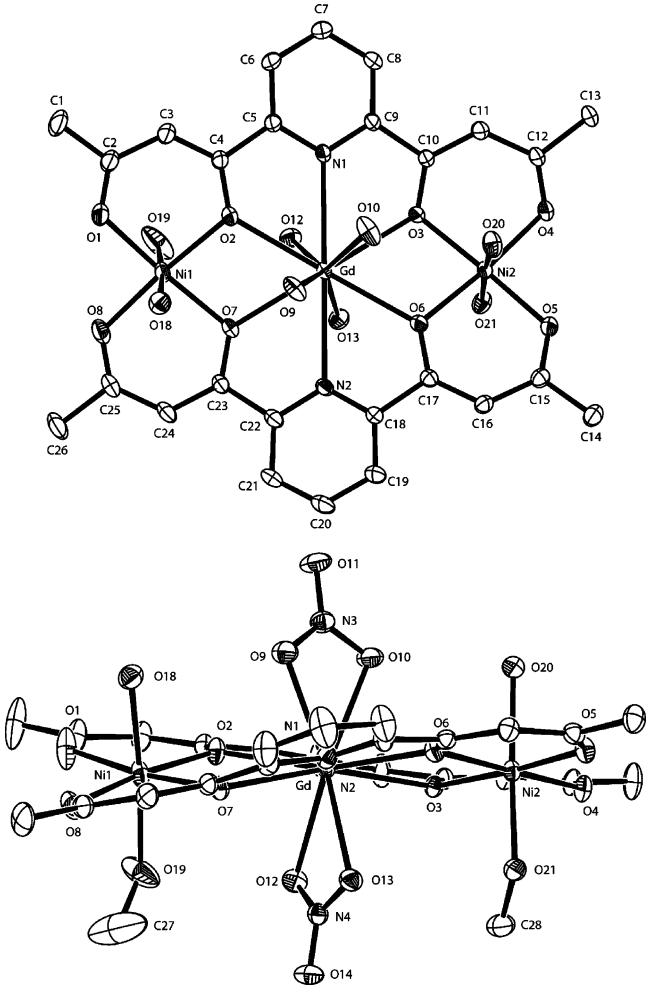


**Figure 2.** ORTEP drawings of $Ni_2Gd$ complex **7-B** (type B).

**Type D. $[Ni_2Ln(L)_2(NO_3)_2(H_2O)(MeOH)_3]NO_3 \cdot Et_2O \cdot MeOH$ (Ln = Ho (10), Er (11), Tm (12), Yb (13), and Lu (14)).** This type crystallizes in the triclinic system of $P\bar{1}$. The structure of **14** is shown in Figure 4 as an example. The $[Ni_2Lu(L)_2]$ core shows a large distortion with respect to two $L^{2-}$ ligands; the dihedral angle ($\phi_{Ln}$) is 43.6°. Two didentate nitrate groups coordinate to the Lu ion, affording a 10-coordinate environment about the metal. The two $Ni^{II}$ ions are not equivalent; Ni(1) has two MeOH molecules at the apical sites, whereas Ni(2) has one water and one MeOH molecule at the apical sites.

The structural data of the type D complexes are included in Table 3. The $\phi_{Ln}$ value varies from 42.6 to 43.6° and increases in the order **10** < **11** < **12** < **13** < **14**. The average Ln−N, Ln−O(L), and Ln−O(nitrate) bond distances decrease in this order. In contrast, the average Ni−O distance slightly increases relative to those of types A−C.

It is obvious from the above crystallographic studies that the size of the $Ln^{III}$ ion is a dominant factor determining the trinuclear core structure (Table 3). Large $La^{III}$−$Nd^{III}$ ions (ionic radius 1.06−0.99 Å) preferentially afford type A, and subsequent $Sm^{III}$−$Gd^{III}$ ions (0.96−0.94 Å) afford both type A and type B. Type C is produced with $Gd^{III}$−$Dy^{III}$ ions of medium size (0.94−0.91 Å), and type D is produced with small $Ho^{III}$−$Lu^{III}$ ions (0.89−0.85 Å). The $[Ni_2Ln(L)_2]$ core is essentially coplanar in type A, whereas it shows a distortion ($\phi_{Ln}$) in types B, C, and D in the increasing order B < C < D. This distortion is the necessary result when the central $N_2O_4$ cavity accommodates a small $Ln^{III}$ ion while maintaining the terminal Ni geometry with ordinary bond distances. The Ln−N, Ln−O(L), and Ln−O(nitrate) bond distances shorten in the order A > B ≈ C > D. The distortion of the trinuclear core also accompanies a distortion about the terminal Ni ($\phi_{Ni}$); the average dihedral angle between the least squares planes defined by Ni and four O atoms increases in the order A (0°) < B (34.47°) < C (47.73°) < D (66.08°). However, the average Ni−O bond distance is practically independent of the Ln ions and falls in the range of 2.031 ± 0.008 Å. That is, the terminal Ni ions keep their geometries while allowing an optimal coordination environment for the central Ln ion.

It is useful to compare the structures of the $Ni_2Ln$ complexes with those of the analogous $Cu_2Ln$ complexes.[17a] In the latter complexes, the bis(1,3-diketonato)$Cu^{II}$ moiety prefers a planar geometry irrespective of the kind of Ln ion. Furthermore, the Cu−N and Cu−O(L) bonds are short, relative to the corresponding bonds of the $Ni_2Ln$ complexes. For these reasons, the $[Cu_2Ln(L)_2]$ core is nearly coplanar except for a slight displacement of the central Ln from the $N_2O_4$ hexagonal base.

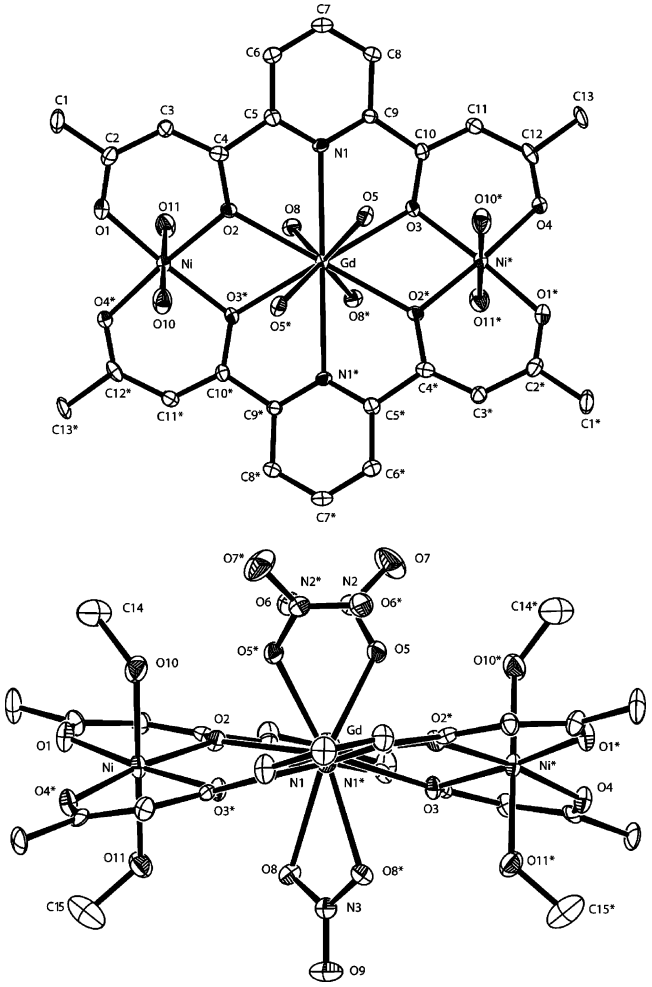


**Figure 3.** ORTEP drawings of $Ni_2Gd$ complex **7-C** (type C).

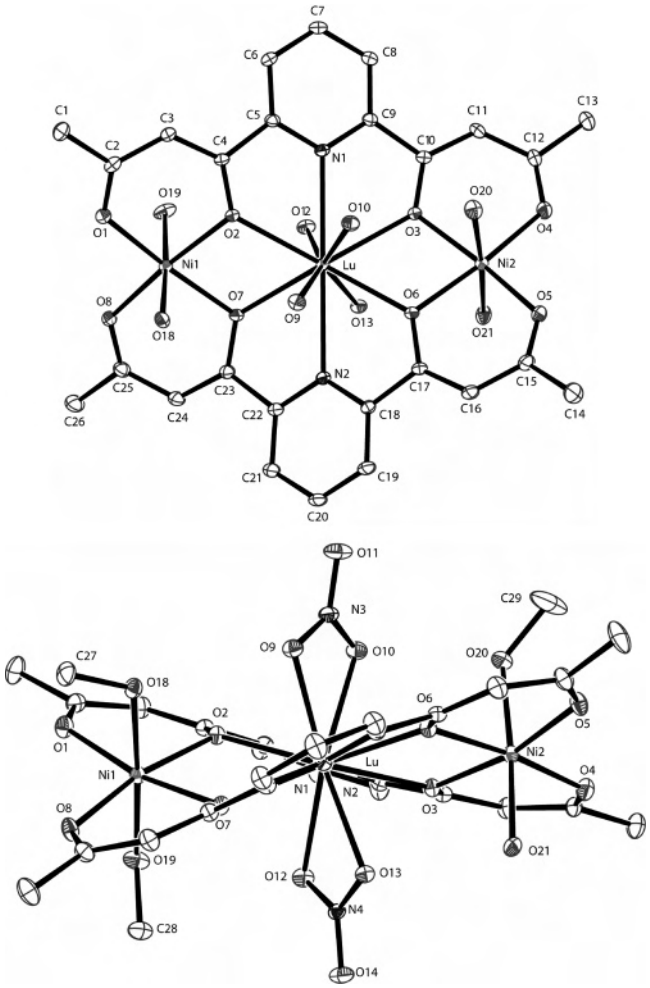


**Figure 4.** ORTEP drawings of $Ni_2Lu$ complex **14** (type D).

**Magnetic Properties. 1′−14′** were used for magnetic studies in the temperature range of 2−300 K under an applied field of 500 Oe. The magnetic properties are discussed in three groups. **1′** and **14′** (group I) have a diamagnetic $Ln^{III}$ ion, so these complexes serve to evaluate the magnetic interaction between the terminal $Ni^{II}$ ions through the $Ln^{III}$ ion. $Ni_2Gd$ complex **7′** is the only member of group II for which the theoretical evaluation of the $Ni^{II}-Ln^{III}$ interaction is possible, because $Gd^{III}$ has no orbital angular momentum. The remaining complexes, **2′−6′** and **8′−13′** (group III), have a Ln ion with a first-order angular momentum. The magnetic nature of the $Ni^{II}-Ln^{III}$ interaction of this group was evaluated in comparison with **1′** ($Ni_2La$) and analogous $Zn_2Ln$ complexes. The $\chi_M T$ versus $T$ plots of the $Zn_2Ln$ analogs and the magnetization curve for **1′−14′** and the $Zn_2Ln$ analogs at 2 K are given in Figures S4−S5 and S8−S9.

**Group I (1′ and 14′).** The $\chi_M T$ versus $T$ curve of **1′** is given in Figure 5. The effective magnetic moment is 2.51 emu $mol^{-1}$ K at room temperature, and the moment decreased with decreasing temperature to 1.06 emu $mol^{-1}$ K at 2 K. Complex **14′** also shows a similar $\chi_M T$ versus $T$ curve (2.43 emu·$mol^{-1}$·K at 300 K and 1.01 emu $mol^{-1}$ K at 2 K. See the inset). Magnetic analyses were carried out using the magnetic susceptibility expression (eq

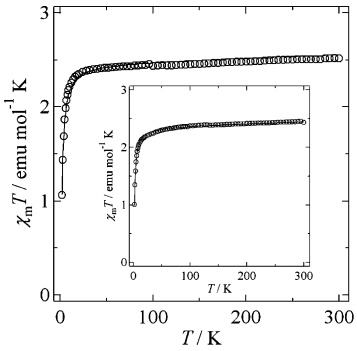


**Figure 5.** $\chi_M T$ versus $T$ plots of **1′** (inset for **14′**). The solid lines represent the theoretical curve (text).

1) based on the isotropic Heisenberg model ($\hat{H} = -2JS_{Ni1} \cdot S_{Ni2}$),

$$\chi_M = \left(\frac{2Ng_{Ni}{}^2\beta^2}{kT}\right)\left(\frac{5\exp(6x) + \exp(2x)}{5\exp(6x) + 3\exp(2x) + 1}\right) + N\alpha \quad \text{with } x = \frac{J}{kT} \quad (1)$$

In this expression, $N$ is Avogadro's number, $g$ is the Landé $g$ factor, $\beta$ is the Bohr magneton, $k$ is the Boltzmann constant, $J$ is the exchange integral, $T$ is the absolute temperature, and $N\alpha$ is the temperature-independent para-

magnetism. Here, other small magnetic contributions (intermolecular interaction, single ion zero-field splitting, etc.) are included in the parameter $J$ for simplicity. As shown by the solid line in Figure 5, the $\chi_M T$ versus $T$ curve of **1′** can be simulated by eq 1 using the best-fit parameters of $J = -0.63$ cm$^{-1}$, $g = 2.22$, and $N\alpha = 320 \times 10^{-6}$ emu·mol$^{-1}$. The discrepancy factor $R(\chi_M)$ defined by eq 2 was $1.49 \times 10^{-2}$, and the discrepancy factor $R(\mu_{eff})$ defined by eq 3 was $6.37 \times 10^{-3}$.

$$R(\chi_M) = [\sum(\chi_{obsd} - \chi_{calcd})^2/\sum(\chi_{obsd})^2]^{1/2} \quad (2)$$

$$R(\mu_{eff}) = [\sum(\mu_{eff_{obsd}} - \mu_{eff_{calcd}})^2/\sum(\mu_{eff_{obsd}})^2]^{1/2} \quad (3)$$

Similarly, the $\chi_M T$ versus $T$ curve of **14′** can be reproduced by eq 1 using the best-fit parameters of $J = -0.65$ cm$^{-1}$, $g = 2.17$, and $N\alpha = 320 \times 10^{-6}$ emu·mol$^{-1}$ ($R(\chi_M) = 1.06 \times 10^{-2}$ and $R(\mu_{eff}) = 3.28 \times 10^{-3}$). It is notable that **1′** and **14′** have similar exchange integrals in spite of a large difference in the $\phi_{Ni}$ value. This fact suggests that the antiferromagnetic contribution in these complexes is hardly affected by the central Ln ion, a distortion in the $[Ni_2Ln(L)_2]$ core, and the intermolecular structure.

**Group II (7′).** The $\chi_M T$ versus $T$ curve of **7′** is shown in Figure 6. The effective magnetic moment at room temperature is 10.70 emu·mol$^{-1}$·K, which is close to the spin-only value (9.88 emu·mol$^{-1}$·K) for two magnetically isolated $Ni^{II}$ and one $Gd^{III}$ ions. The magnetic moment increased with decreasing temperature to reach 16.22 emu·mol$^{-1}$·K at 3 K. This value is close to the spin-only magnetic moment for $S_T = {}^{11}/_2$ (17.88 emu·mol$^{-1}$·K) resulting from the ferromagnetic coupling of two $Ni^{II}$ and one $Gd^{III}$ ions. The spin Hamiltonian for the linear $Ni^{II}Gd^{III}Ni^{II}$ system is given as follows:

$$\hat{H} = -2J(S_{Ni1}\cdot S_{Gd} + S_{Ni2}\cdot S_{Gd}) - 2J'S_{Ni1}\cdot S_{Ni2} \quad (4)$$

where $J$ is the exchange integral between the adjacent $Ni^{II}$ and $Gd^{III}$ ions and $J$' is the exchange integral between the terminal $Ni^{II}$ ions including other magnetic contributions. The magnetic susceptibility expression for this system is given by eq 5:

$$\chi_M = \frac{N\beta^2}{4kT}\cdot\frac{FU}{FD} + N\alpha$$

$$FU = 286[(52g_{Ni} + 91g_{Gd})/143]^2 \exp(32x + 6y) + 165[(30g_{Ni} + 69g_{Gd})/99]^2 \exp(21x + 6y) + 84[(12g_{Ni} + 51g_{Gd})/63]^2 \exp(12x + 6y) + 35[(-2g_{Ni} + 37g_{Gd})/35]^2 \exp(5x + 6y) + 10[(-12g_{Ni} + 27g_{Gd})/15]^2 \exp(6y) + 165[(22g_{Ni} + 77g_{Gd})/99]^2 \exp(25x + 2y) + 84[(4g_{Ni} + 59g_{Gd})/63]^2 \exp(16x + 2y) + 35[(-10g_{Ni} + 45g_{Gd})/35]^2 \exp(9x) + 84g_{Gd}^2 \exp(18x)$$

$$FD = 6 \exp(32x + 6y) + 5 \exp(21x + 6y) + 4 \exp(12x + 6y) + 3 \exp(5x + 6y) + 2 \exp(6y) + 5 \exp(25x + 2y) + 4 \exp(16x + 2y) + 3 \exp(9x + 2y) + 4 \exp(18x)$$

$$\text{with } x = \frac{J}{kT} \qquad y = \frac{J'}{kT} \quad (5)$$

In this expression, $g_{Ni}$ and $g_{Gd}$ are the $g$ factors associated with $Ni^{II}$ and $Gd^{III}$, respectively. In practice, magnetic simulations were carried out using $g_{Ni} = 2.20$ and $J' = -0.64$ cm$^{-1}$ (the mean values for **1′** and **14′**). As indicated by the solid line in Figure 6, the cryomagnetic property of **7′** was reproduced by eq 5 using the best-fit parameters of $J = +0.79$ cm$^{-1}$, $g_{Gd} = 2.02$, and $N\alpha = 320 \times 10^{-6}$ emu·mol$^{-1}$. The discrepancy factors, $R(\chi_M)$ and $R(\mu_{eff})$, were $1.46 \times 10^{-1}$ and $1.65 \times 10^{-2}$, respectively. The result clearly demonstrates a ferromagnetic interaction between the adjacent $Ni^{II}$ and $Gd^{III}$ ions. The magnetization curve adds support to the ferromagnetic interaction between the $Ni^{II}$ and $Gd^{III}$ ions of **7′** (Figure S1). The magnetization per $Ni_2Gd$ sharply increases with applied magnetic field to reach 11.42 $N\beta$ under 5 T, and the $M$ versus $H$ curve exceeds the Brillouin function for $S = {}^2/_2 + {}^7/_2 + {}^2/_2$, which corresponds to two $Ni^{II}$ and one $Gd^{III}$ magnetically isolated ions. However, it lies below the curve for $S = {}^{11}/_2$ arising from the parallel alignment of the spins of two $Ni^{II}$ and one $Gd^{III}$ ions (Figure S1). It is suggested that a ferromagnetic interaction between $Ni^{II}$ and $Gd^{III}$ ions and weak antiferromagnetic contributions exist.

**Group III (2′−6′ and 8′−13′).** The magnetic moments of **2′−6′** and **8′−13′** at room temperature are summarized in Table 4, along with the magnetic moments of **1′**, **7′**, and **14′**. In Table 4 are also given the magnetic moments calculated by eq 6 for two $Ni^{II}$ and one $Ln^{III}$ magnetically isolated ions,

$$\chi_M T_{calcd} = \frac{2 \times g_{Ni}^2 S_{Ni}(S_{Ni} + 1) + g_J^2 J(J + 1)}{8} \quad (6)$$

In this equation $g_J$ is the $g$ factor of the ground $J$ terms of $Ln^{III}$ and is expressed as

$$g_J = \frac{3}{2} + \frac{S(S + 1) - L(L + 1)}{2J(J + 1)} \quad (7)$$

In the calculation of $\chi_M T_{calcd}$, the $g_{Ni}$ was fixed at 2.20 (the average $g$ value of **1′** and **14′**). Each magnetic moment of **2′−5′** and **8′−13′** is close to the respective calculated moment, indicating that the $Ni^{II}-Ln^{III}$ magnetic interaction

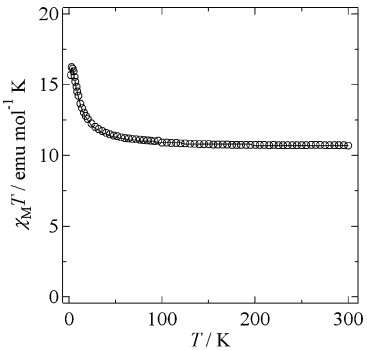


**Figure 6.** $\chi_M T$ versus $T$ plots of **7′**. The solid lines represent the theoretical curve (text).

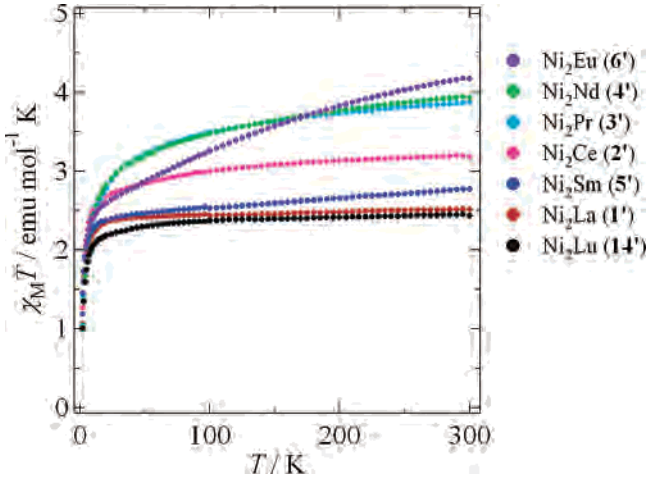


**Figure 7.** $\chi_M T$ versus $T$ plots for **1′**−**6′** and **14′**. **1′** (red), **2′** (pink), **3′** (light blue), **4′** (greenish yellow), **5′** (blue), **6′** (purple), **14′** (black).

**Table 4.** Observed and Calculated Magnetic Moments for **1′**−**14′** at 300 K

| complex | | no. of f electron(s) | $g_J$ | $\chi_M T$ | $\chi_M T_{calcd}$[a] |
|---|---|---|---|---|---|
| $Ni_2La$ | (**1′**) | 0 | 0 | 2.51 | 2.42 |
| $Ni_2Ce$ | (**2′**) | 1 | $^6/_7$ | 3.18 | 3.22 |
| $Ni_2Pr$ | (**3′**) | 2 | $^4/_5$ | 3.88 | 4.02 |
| $Ni_2Nd$ | (**4′**) | 3 | $^8/_{11}$ | 3.93 | 4.06 |
| $Ni_2Sm$ | (**5′**) | 5 | $^2/_7$ | 2.77 | 2.51 |
| $Ni_2Eu$ | (**6′**) | 6 | 0 | 4.18 | 2.42 |
| $Ni_2Gd$ | (**7′**) | 7 | 2 | 10.70 | 10.30 |
| $Ni_2Tb$ | (**8′**) | 8 | $^3/_2$ | 14.18 | 14.23 |
| $Ni_2Dy$ | (**9′**) | 9 | $^4/_3$ | 16.39 | 16.59 |
| $Ni_2Ho$ | (**10′**) | 10 | $^5/_4$ | 16.65 | 16.48 |
| $Ni_2Er$ | (**11′**) | 11 | $^6/_5$ | 13.29 | 13.90 |
| $Ni_2Tm$ | (**12′**) | 12 | $^7/_6$ | 9.33 | 9.57 |
| $Ni_2Yb$ | (**13′**) | 13 | $^8/_7$ | 4.85 | 4.99 |
| $Ni_2Lu$ | (**14′**) | 14 | 0 | 2.43 | 2.42 |

[a] $\chi_M T_{calcd}$ values were obtained by eq 6 using $g_{Ni} = 2.20$.

is weak, if it operates at all (Table 4). A subnormal magnetic moment of **6′** is associated with $Eu^{III}$ that has the thermally accessible $J = 1$ and $J = 2$ excited terms.

The $\chi_M T$ versus $T$ curves of **2′**−**6′** and **8′**−**13′** are shown in Figures 7 and 8, respectively. For comparison, the $\chi_M T$ versus $T$ curves of **1′** and **14′** are included in Figure 7 and the $\chi_M T$ versus $T$ curve of **7′** is included in Figure 8.

The $\chi_M T$ values of **2′**−**6′** decrease with decreasing temperature as well as **1′** and **14′**. The $\chi_M T$ versus $T$ curve of **6′** shows a rather rapid decrease because of the depopulation of the thermally accessible $J = 1$ and $J = 2$ terms of $Eu^{III}$. The $\chi_M T$ values of **10′**−**13′** also decrease with decreasing temperature, whereas the $\chi_M T$ values of **8′** and **9′** increase at low temperature. Apparently, the $Ni^{II}$−$Tb^{III}$ interaction in **8′** and the $Ni^{II}$−$Dy^{III}$ interaction in **9′** are ferromagnetic, whereas it is unclear from Figures 7 and 8 whether any magnetic interaction operates between $Ni^{II}$ and $Ln^{III}$ ions in **2′**−**6′** and **10′**−**13′**.

The cryomagnetic properties of **2′**−**6′** and **8′**−**13′** are governed by three factors: the thermal population of the Stark components of $Ln^{III}$, the $Ni^{II}\cdots Ni^{II}$ interaction (including intermolecular interaction), and the $Ni^{II}$−$Ln^{III}$ interaction. To evaluate more explicitly the nature of the $Ni^{II}$−$Ln^{III}$ interaction, we adopted the empirical method reported by

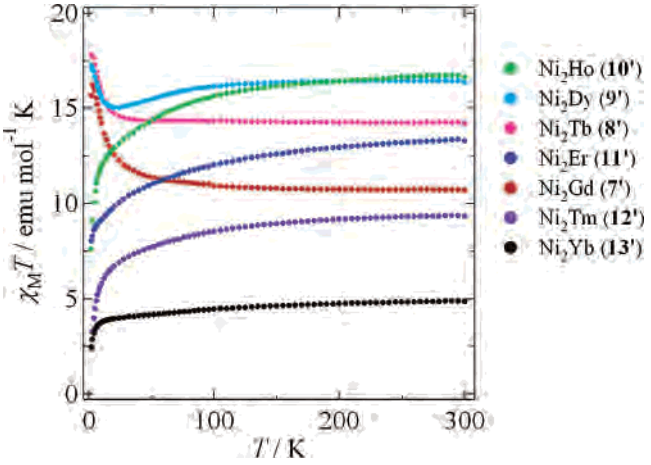


**Figure 8.** $\chi_M T$ versus $T$ plots for **7′**−**13′**. **7′** (red), **8′** (pink), **9′** (light blue), **10′** (greenish yellow), **11′** (blue), **12′** (purple), **13′** (black).

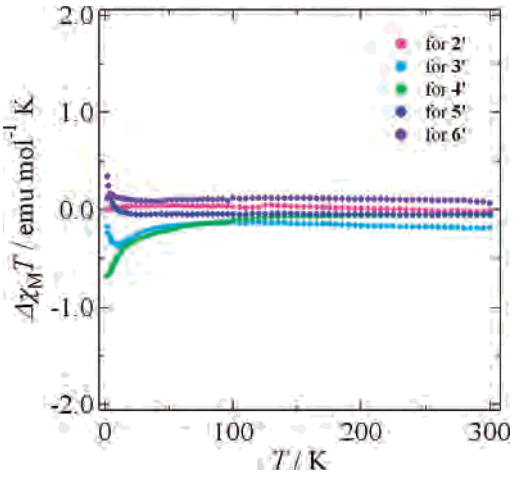


**Figure 9.** $\Delta\chi_M T$ versus $T$ plots for **2′**−**6′**. **2′** (pink), **3′** (light blue), **4′** (greenish yellow), **5′** (blue), **6′** (black).

Kahn et al.[13b] and used a modified equation, $\Delta\chi_M T = \chi_M T(Ni_2Ln) - \chi_M T(Zn_2Ln) - \chi_M T(Ni_2La)$, as an indication of ferromagnetic ($\Delta\chi_M T > 0$) or antiferromagnetic ($\Delta\chi_M T < 0$) interaction, where $\chi_M T(Ni_2Ln)$, $\chi_M T(Zn_2Ln)$, and $\chi_M T(Ni_2La)$ are the $\chi_M T$ values of a $Ni_2Ln$ complex, its reference $Zn_2Ln$ complex and **1′**, respectively. Here, we identify the trinuclear core structure of $Zn_2Ln$ compounds with those of $Ni_2Ln$ compounds and ignore the differences in intermolecular structures between them (Figures S2, S3). This treatment is based on the assumption that the $Ni^{II}$−$Ni^{II}$ interaction is hardly affected by the $Ln^{III}$ ion throughout **2′**−**13′**, which is confirmed by the results of group I. The $\Delta\chi_M T$ versus $T$ curves for **2′**−**6′** and **7′**−**11′** are given in Figures 9 and 10, respectively. (The curves for **12′** and **13′** are not given because the reference $Zn_2Tm$ and $Zn_2Yb$ complexes have not been obtained in sufficient purity.)

The $\Delta\chi_M T$ values for **2′**−**6′** fall in the range of −0.179 to 0.068 emu·mol$^{-1}$·K at room temperature. In the case of $Ni_2$-Nd compound **4′**, $\Delta\chi_M T$ values decrease with decreasing temperature down to 2 K (Figure 9), which clearly demonstrates the operation of the antiferromagnetic interaction between the $Ni^{II}$ and $Nd^{III}$ ions. $Ni_2Pr$ compound **3′** also shows essentially antiferromagnetic behavior except for a small increase below 6 K. The increase would reflect an

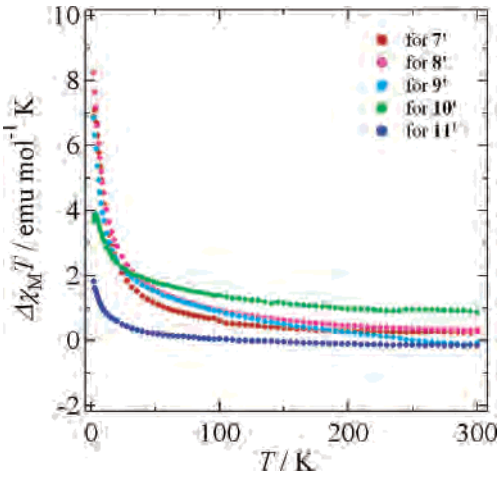


**Figure 10.** $\Delta\chi_M T$ versus $T$ plots for **7′**−**11′**. **7′** (red), **8′** (pink), **9′** (light blue), **10′** (greenish yellow), **11′** (blue).

effect of slight commingling of a paramagnetic impurity or a difference of intermolecular interaction between **3′** and **1′**. The $\Delta\chi_M T$ values of $Ni_2Ce$ compound **2′** are almost zero in the range until 18 K, and then slightly decrease, which could be regarded as an effect of a very weak antiferromagnetic interaction between $Ni^{II}$ and $Ce^{III}$ ions. In the case of $Ni_2Sm$ (**5′**) and $Ni_2Eu$ (**6′**), the $\Delta\chi_M T$ versus $T$ plots do not clearly show the decrease. The $\Delta\chi_M T$ values of **5′** are smaller than zero until 18 K; however, they increase below 18 K and reach 0.344 emu·mol$^{-1}$·K at 2 K. Nonetheless, the $\Delta\chi_M T$ values of **6′** are larger than zero until 2 K with a small increase. The results of **5′** and **6′** would be affected by the following factors: (1) The ligand field effect on the central $Ln^{III}$ ions in **5′** and **6′** is different from that of $Zn_2Ln$ analogues because the aqua complexes **5′** and **6′** are essentially mixtures of types A and B in the crystalline form. (2) $Sm^{III}$ and $Eu^{III}$ have relatively low excited states, and their magnetic behaviors reflect the structural differences between $Ni_2Ln$ and $Zn_2Ln$ complexes. In the case of **7′**−**11′**, the $\Delta\chi_M T$ values are generally larger than zero over the whole temperature range, which definitely indicates ferromagnetic interaction between the adjacent $Ni^{II}$ and $Ln^{III}$ ions (Figure 10). These results are consistent with Kahn's predictions.[13e] The magnetization value of **1′**−**14′** at 2 K under an applied field of 50 kOe also supports the magnetic interaction (Figures S6−S9).

## Conclusions

A series of $Ni^{II}_2Ln^{III}$ complexes of a linear NiLnNi structure were systematically derived from 2,6-di(acetoacetyl)-pyridine ($H_2L$). Eighteen structures were determined by single-crystal X-ray diffraction analysis, and the complexes were classified into four different types: $[Ni_2Ln(L)_2(NO_3)_2(MeOH)_4]NO_3$·MeOH (type A: Ln = La (**1**), Ce (**2**), Pr (**3**), Nd (**4**), Sm (**5-A**), Eu (**6-A**), Gd (**7-A**)); $[Ni_2Ln(L)_2(NO_3)_2(H_2O)_2(MeOH)_2]NO_3$·$2H_2O$·MeOH (type B: Ln = Sm (**5-B**), Eu (**6-B**), Gd (**7-B**)); $[Ni_2Ln(L)_2(NO_3)_3(MeOH)_4]$ (type C: Ln = Gd (**7-C**), Tb (**8**), Dy (**9**)); and $[Ni_2Ln(L)_2(NO_3)_2(H_2O)(MeOH)_3]NO_3$·$Et_2O$·MeOH (type D: Ln = Ho (**10**), Er (**11**), Tm (**12**), Yb (**13**), Lu (**14**)). The structural types A−D consist of the linear $[Ni_2Ln(L)_2]$ core and exogenous donor groups (nitrate ions, methanol, water), and each Ni has a six-coordinate geometry together with two molecules of methanol or water, and Ln has a 10-coordinate geometry together with two or three nitrate groups. The $[Ni_2Ln(L)_2]$ core is essentially coplanar in type A, but shows a distortion in types B, C, and D with increasing order of distortion B < C < D. The distortion results when the central $N_2O_4$ cavity accommodates a small Ln ion while maintaining the Ni geometry in the ordinary bond distance. The crystals of **1**−**14** were efflorescent and converted into $[Ni_2Ln(L)_2(NO_3)_3(H_2O)_4]$·$nH_2O$ (**1′**−**14′**). Magnetic properties were studied using **1′**−**14′**. **1′** ($Ni_2La$) and **14′** ($Ni_2Lu$) indicate a weak antiferromagnetic interaction between the terminal $Ni^{II}$. The $Ni^{II}$−$Ln^{III}$ interaction is weakly antiferromagnetic in **2′** ($Ni_2Ce$), **3′** ($Ni_2Pr$), and **4′** ($Ni_2Nd$); however, interactions in **5′** ($Ni_2Sm$) and **6′** ($Ni_2Eu$) were not clearly established by the numerical approach. Nonetheless, the $Ni^{II}$−$Ln^{III}$ ferromagnetic interaction in **7′** ($Ni_2Gd$), **8′** ($Ni_2Tb$), **9′** ($Ni_2Dy$), **10′** ($Ni_2Ho$), and **11′** ($Ni_2Er$) was clearly demonstrated. We presume the $Ni^{II}$−$Tm^{III}$ interaction of **12′** and the $Ni^{II}$−$Yb^{III}$ interaction of **13′** also to be ferromagnetic, analogous to the magnetic interaction in **7′**−**11′**.

**Acknowledgment.** This work was supported by a Grant-In-Aid for Science Research in a Priority Area "Chemistry of Coordination Space (no. 16074209)" and Core Research for Evolutional Science and Technology (CREST), Japan Science and Technology Corporation (JST), Japan.

**Supporting Information Available:** Crystallographic data for **1**−**14** (CCDC 623149−623166). $M$ versus $H$ curve for **7′** (Figure S1) with Brillouin functions. Crystal structures of $Zn_2La$ and $Zn_2Gd$ complexes (Figures S2, S3). $\chi_M T$ versus $T$ plots of $Zn_2Ln$ complexes (Figures S4, S5). $M$ versus $H$ curve of $Ni_2Ln$ complexes **1′**−**14′** (Figures S6, S7). $M$ versus $H$ curve of $Zn_2Ln$ complexes (Figures S8, S9). This material is available free of charge via the Internet at http://pubs.acs.org.

IC0619153